Jurnal Elektronika dan Telekomunikasi (JET), Vol. 24, No. 1, August 2024, pp. 46-51
Accredited by KEMDIKBUDRISTEK, Decree No: **158/E/KPT/2021**
doi: 10.55981/jet.642

Ground Penetrating Radar Data Inversion Using Dual-Input Convolutional Autoencoder for Ferroconcrete Inspection

Budiman P. A. Rohman [a, b, *], Masahiko Nishimoto [c], Ratna Indrawijaya [a], Dayat Kurniawan [a], Iman Firmansyah [a], Bagus Edi Sukoco [a]

[a]Research Center for Telecommunication
National Research and Innovation Agency (BRIN)
KST Samaun Samadikun, Jl. Sangkuriang
Bandung, Indonesia
[b]School of Electrical Engineering
Telkom University
Jl. Telekomunikasi 1
Bandung, Indonesia
[c]Faculty of Advanced Science and Technology
Kumamoto University
2-39-1 Kurokami, Chuo Ward
Kumamoto, Japan

Abstract

Ground penetrating radar (GPR) is a non-destructive tool for exploring an underground object. Currently, GPR is also considered for reinforced concrete inspection. However, the image produced by GPR cannot be easily interpreted. Besides, the large observation of building concrete inspection motivates researchers to fasten and ease radar image interpretation. Thus, this research proposes a new method to translate the GPR scattering data image to its internal structure visualization. The proposed method employs a convolutional autoencoder model using amplitude and phase radar data as input of the algorithm. As an evaluation, in this stage, we perform numerical analysis by using finite-difference time-domain-based synthetic data that considers three cases: concrete with rebar, concrete with crack, and concrete with rebar and crack. All those cases are simulated with randomized dimensions and positions that are possible in real applications. Compared with the baseline method, our method shows superiority, especially in the semantic segmentation perspective. The parameter size of the proposed model is also much smaller, around one-third of the previous method. Therefore, the method is feasible enough to be implemented in real applications addressing an automatic internal structure reinforced concrete visualization.

Keywords: radar, ground penetrating radar, wave inversion, full wave inversion, deep learning, machine learning, autoencoder, convolutional neural networks.

I. INTRODUCTION

Ground penetrating radar (GPR) is a sensing technology that utilizes electromagnetic waves to investigate information about subsurface objects. When electromagnetic waves travel to the ground, the buried object partially reflects them. These reflected waves are subsequently processed and analyzed to locate the object and ascertain its characteristics. GPR has been applied in various fields, including geophysics, geology, archeology, civil engineering, and humanitarian demining [1], [2]. Of particular interest to researchers currently is the latest application of GPR: non-destructive inspection of concrete structures, as referenced in [3], [4] and [5]. However, it is challenging to interpret the recorded data and images from the GPR. Some advanced and complex processing is required. Thus, simple and lightweight data processing is required to fasten and ease the non-destructive inspection of data acquisition and interpretation.

The Full Waveform Inversion (FWI) is the standard method to identify the buried object from GPR signals. Some of the research that proposes that method is as follows. In 2012, Busch et al. proposed the quantitative conductivity and permittivity estimation using FWI [6]. In 2014, Forte et al. analyzed the velocity from common offset GPR data inversion applied in the synthetic and real data [7]. A spectral inversion method on GPR data was proposed by Huang et al. to determine the parameters of subsurface layers [8]. In 2019, Jazayeri made reinforced concrete mapping using FWI of GPR data [9].

Artificial intelligence algorithms, especially Deep Learning (DL), are currently popular. This algorithm can make a black box that mimics any input and output transformation. The use of DL algorithms on the ultrawideband radar image data to reconstruct the internal structure of material became the concern of many researchers. Many of them use deep learning to detect, classify, and recognize the buried object in the structure [10]-[14]. However, currently, researchers are using this technique as a new approach to the radar response inversion problem. The inversion of radar images using

* Corresponding Author.
Email: budi057@brin.go.id
Received: May 20, 2024 ; Revised: June 27, 2024
Accepted: July 09, 2024 ; Published: August 31, 2024

deep learning algorithms, such as Enc-Dec, U-Net, and GAN, was conducted by Alvarez et al. [15]. The convolutional-to-trace network has been proposed to reconstruct the image and tunnel lining structure [16]. Ji et al. proposed a deep neural network for inverting the permittivity of GPR data [17]. The use of a convolutional neural network in the SegNet architecture to segment the defect of the buried object in the lining tunnel based on its permittivity values has been proposed by Yang et al. [18]. However, implementing those methods in the real GPR data still has drawbacks and limitations.

In this proposal, we develop a new machine-learning structure to improve the performance of the previous method. Inspired by the valuable information carried by the radar signal phase [8]-[9] and the success of the previous research in the buried shape reconstruction using this feature [10], we use both amplitude and phase images of the GPR B-scan data in this study. In this paper, we propose a DL-based inversion method that concurrently employs the amplitude and phase of the reflection signal, aiming at an accurate and light computation model. By combining information carried by amplitude and phase with an appropriate technique, we hypothesize that the developed model can perform better inversion. Besides, from this study, we can also obtain different perspectives on the exploration of the phase information of radar data for image inversion. As an evaluation, we focus on applying reinforced concrete inspection employing synthetic data based on the finite-difference time-domain method. We use the method from [18] as the performance and model complexity evaluation baseline.

The remainder of this paper is organized as follows: Section II briefly explains the proposed method, followed by the numerical analysis setup in Section III. The result of the analysis is explained in section IV. Then, the conclusion of this study is described in section V.

II. PROPOSED METHOD

A. Ferroconcrete Inspection

In the concrete inspection using GPR (see Figure 1), the GPR works by emitting an electromagnetic pulse through the emission antenna. The radar waves propagate in the concrete at a speed that depends on the electrical properties of the media. The receiving antenna receives electric fields generated by internal objects such as rebar or crack/void according to the time. The electrical properties that significantly affect the GPR recorded signal are permittivity (ε) and conductivity (σ). Electrical conductivity conveys the current density information generated by an external electric field, while permittivity is a complex-valued attribute indicating the medium's susceptibility to polarization by external electric fields. The complex permittivity (ε_c) is defined about ε and σ as (1),

$$\varepsilon_c = \varepsilon - j\frac{\sigma}{\omega} = \varepsilon' - j\varepsilon'' \tag{1}$$

where the real part, $\varepsilon' = \varepsilon$, corresponds to the dielectric constant, while the imaginary part, $\varepsilon'' = \frac{\sigma}{\omega}$, represents the loss factor, indicative of energy dissipation due to absorption. The dielectric constant or relative permittivity, ε_r. This value is obtained by dividing it by the free space permittivity, $\varepsilon_0 = 8.854 \times 10^{-12}$ F/m, expressed by (2).

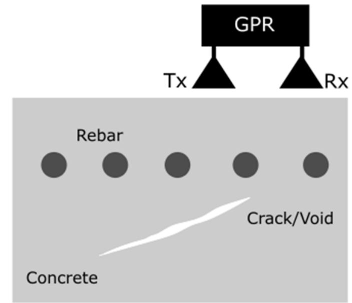

Figure 1. The process of ferroconcrete inspection.

$$\varepsilon_r = \frac{\varepsilon}{\varepsilon_0} \tag{2}$$

The alteration in this dielectric constant value is primarily induced by the water content, which causes its high dielectric constant and substantial loss factor. To generalize the condition of concrete, in this study, we simulate the dielectric constant in the range of 6 to 8.

B. Deep Learning Method

DL constitutes a sector within machine learning that constructs a nonlinear parametrized mapping by processing through multiple layers to extract high-level features. At the heart of this algorithm is the artificial neural network, which simulates human neurons [19]. If f is defined as a function of DL, then the predicted value can be seen in (3),

$$\boldsymbol{Y_P} = f(\boldsymbol{X}, \boldsymbol{\theta}) \tag{3}$$

where $\boldsymbol{Y_P}$ denotes the predicted value, $\boldsymbol{X}$ signifies the vector of input data, and $\boldsymbol{\theta}$ symbolizes the parameter set of the DL model, usually consisting of weight and bias values, among other factors. The neural network parameters undergo iterative adjustments during the learning phase to minimize the estimation error between the predicted and target values.

C. Dual Input Convolutional Autoencoder

The autoencoder algorithm is a variation of the feed-forward neural network designed to compress input data into condensed representations and then reconstruct the original input data using the learned compact representations. This algorithm operates within the unsupervised learning paradigm, which aims to make the target values equal to the inputs. This algorithm consists of two symmetric but separate components: the encoder and the decoder. During the training process, parameters are learned to minimize discrepancies between the original data and the reconstructed outputs through backpropagation.

Convolutional autoencoders (CAE) have a similar architectural pattern to classic autoencoders, incorporating encoding and decoding layers. However, unlike autoencoder, which relies on fully connected

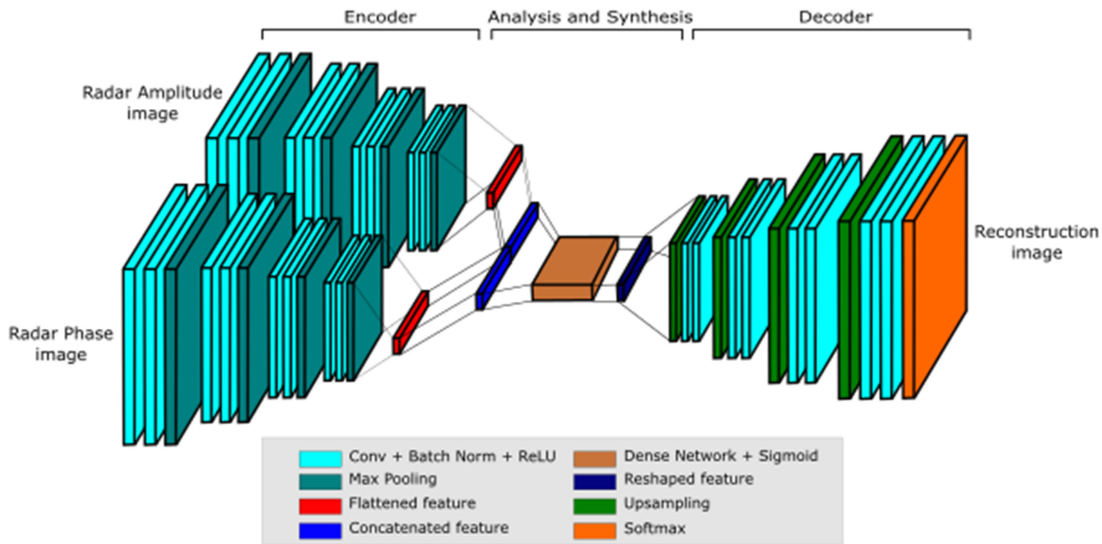

Figure 2. Proposed dual-input convolutional autoencoder.

layers, CAE employs convolutional and max-pooling layers for encoding and decoding. These layers are specifically designed to transform high-dimensional input vectors into lower-dimensional compact feature vectors, with the decoding layers structured using convolutional layers. The main components of this architecture include convolution layers, pooling layers, and fully connected layers. Through the application of the backpropagation algorithm, this process aims to learn spatial hierarchies of features automatically.

In this study, we take the concrete inspection using GPR as a semantic segmentation or pixel categorization problem, which means the algorithm will classify each pixel to the targeted class representing an object (concrete, rebar, or crack). The autoencoder architecture comprises 4 encoding layers from 2 inputs and 4 decoding layers (see Figure 2). We consider amplitude and phase radar images with a size of 160 × 160 pixels as input. The sample of both images can be seen in Figure 3. The encoding convolutional layer filter numbers are 8, 16, 24, and 32, respectively, with a filter size of 15 × 15. Each convolutional layer is followed by a batch normalization layer, Rectified Linear Unit (ReLU) activation unit, and max pooling layer with size 2 × 2. After the fourth layer of the encoding step, the result from both input (amplitude and phase) are flattened to be

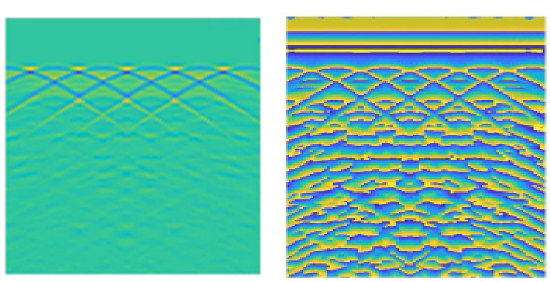

(a) (b)

Figure 3. The amplitude (a) and phase (b) images of GPR data as input of the proposed method.

processed by the fully dense network with a sigmoid activation function.

The next step is a decoding process that also consists of four layers. The first layer consists of the upsampling layer with size 2×2, a convolutional layer with the number 32 and a filter size of 15×15, a batch normalization, and a ReLU activation function. This layer is followed by the other three layers with the same order structure, but their filter numbers of the convolutional layer are 24, 16, and 8, respectively, mirroring the encoder parts.

The final layer consists of one convolutional layer with the filter size 1×1, batch normalization, and a softmax activation function to generate the translated radar data, categorizing each image pixel into a targeted class (concrete, rebar, or crack).

III. Numerical Analysis Setup

A. Dataset

As a dataset, we used a synthetic dataset generated by gprMax, a finite-difference time-domain-based electromagnetic software [20]. The Hertzian dipole antenna is placed above concrete around 1 cm and moves forward with a step of 5 mm to produce a B-scan. Between the transmitter and receiver antenna, there is a range of 4 cm (see Figure 4). The radar employs a monocycle pulse with the center of frequency 2 GHz while the equation of the waveform is defined as (4),

$$W(t) = -2\sqrt{\frac{e}{2\psi}}\psi(t-\omega)e^{-\psi(t-\omega)^2} \qquad (4)$$

where $\psi = 2\pi^2 f^2$, $\omega = \frac{1}{f}$, and f is the radar frequency. The shape of the waveform can be seen in Figure 5.

In this study, we consider three conditions of reinforced concrete: concrete with rebars (Case I); concrete with crack (Case II); and concrete with rebars and crack (Case III). The sample of data is shown in Figure 6. From Table 1, we can see the parameters of the

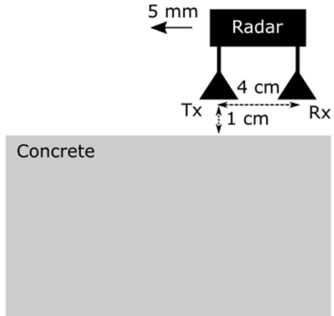

Figure 4. Setup of model for synthetic data generation.

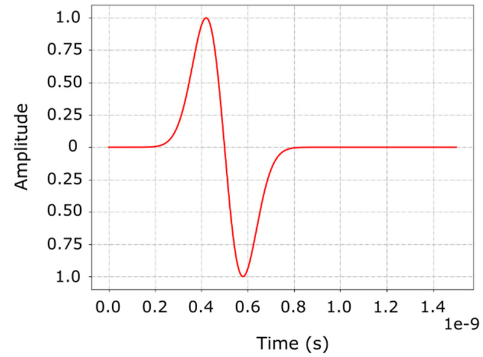

Figure 5. Monocycle pulse excited by GPR.

TABLE 1
MODEL PARAMETERS FOR SYNTHETIC DATA

Component	ε_r	σ	Dimension (cm)
Concrete	6-8	0.0001	width =50, height=49
Rebar (PEC)	1	∞	radius=0.5-1.5, space= 4xR
Crack/Void	1	0	length=5-30, width=0.5-2.0

object, such as relative permittivity (ε_r) and conductivity (σ). The condition of each component is with various depths, various radii, and various spaces (rebars). Each case has 3000 B-scan data: 2000 for training, 500 data for validation, and 500 data for testing. Thus, in this study, we used a total of 9000 data with an equal case distribution.

In this study, we take the semantic segmentation problem as the basis for assessing the effectiveness of the proposed model. We employ four metrics: accuracy, precision, recall, and F1-score. Accuracy is computed by dividing the total number of correct predictions by the sum of true positive and false negative occurrences. This shows the ratio of accurate predictions. Precision measures the accuracy in predicting positive classes. This metric is calculated by dividing the sum of true positive and false positive occurrences by the total number of positive predictions. Recall measures the ratio of correctly predicted positive classes, determined by dividing the sum of true positive and false negative occurrences by the total number of true positive instances. The F1-score represents the weighted average of recall and precision, with a score of 1 indicating optimal performance and 0 indicating the poorest. These metrics can be expressed as (5)-(8),

$$Accuracy = \frac{TP+TN}{TP+FN+TN+FP} \tag{5}$$

$$Precision = \frac{TP}{TP+FP} \tag{6}$$

$$Recall = \frac{TP}{TP+FN} \tag{7}$$

$$F1-score = \frac{2 \times Precision \times Recall}{Precision + Recall} \tag{8}$$

where TP stands for true positives, TN for true negatives, FP for false positives, and FN for false negatives. These four metrics are calculated for each class using a one-vs-rest approach. TP and TN represent cases where the model

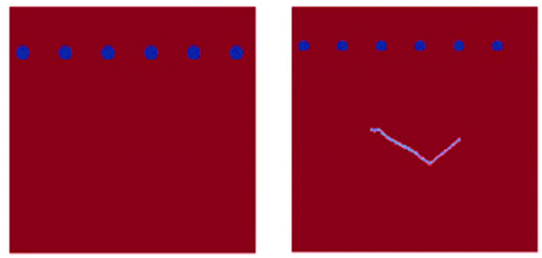

(a) (b)

Figure 6. Sample of simulated model for generating synthetic data: (a) concrete with rebars and (b) concrete with rebars and cracks.

correctly predicted the positive and negative classes. FP denotes cases where the model incorrectly predicted the positive class instead of the negative. In contrast, FN indicates cases where the model incorrectly predicted the negative class instead of the positive.

B. Implementation

The proposed model underwent training and testing on a 64-bit Windows 10 Pro workstation equipped with an Intel Core i7-8700K CPU operating at 3.70 GHz with 12 cores. The computer memory is 32 GB of RAM, and the graphic card is an NVIDIA RTX 3060 GPU. The deep learning model was constructed using TensorFlow and Keras frameworks. During the training phase, a mini-batch size of 8 was utilized alongside a learning rate set at 1^{-2}. The maximum epoch is 100. To prevent overfitting, an early-check mechanism based on validation loss value was integrated into the training process, terminating training when performance ceased to improve, with a delay of 10 epochs.

IV. RESULTS

The proposed method performance is evaluated from three perspectives: model training process, inversion result visualization, and metrics evaluation. A comparison with the existing method was also taken to see the advancement of the proposed method.

A. Model Training

Figure 7 shows the change in the loss curve during data training. It clearly shows that the loss converges around epoch 80 in both training and validation data. This figure also confirms no underfitting or overfitting in the training process.

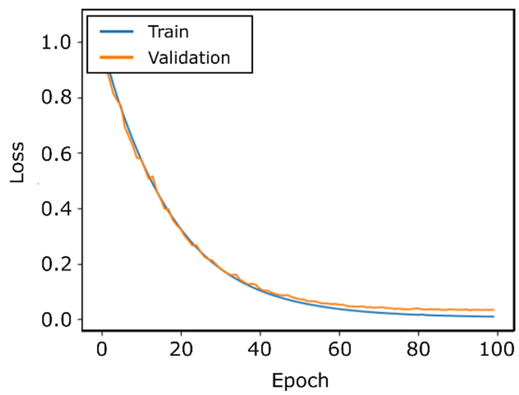

Figure 7. Loss curve during the training process.

B. Data Inversion Visualization

Figure 8 compares inversion results using the baseline and proposed methods. In case I, there is no significant difference in the results between baseline and proposed methods. Thus, in this stage, both methods have relatively equal performance. However, in cases II and III, it can be seen clearly that the proposed method has better performance, especially in the shape and area of the crack. From those two observations, we can conclude that the rebars are easy to detect and invert. The strong reflection from the rebar causes this. Meanwhile, the crack cannot be detected well since the crack reflection is weak, complex, and relatively tight. In case III, the crack reflection signal is also masked by the rebar's, so the reconstruction result is not as accurate as the two previous cases.

C. Metrics Evaluation

The superiority of the proposed method in the inversion results is confirmed further by Table 2. This table shows the performance metrics of both methods from the semantic segmentation perspective. From this table, the proposed method has a higher score in all cases and metrics. Although the difference is relatively small, those results still should be considered since the metrics calculate each pixel's categorization results, and the majority of the pixel of the image is concrete. Thus, from this evaluation, we can confirm confidently that the method performs better than the baseline.

To further evaluate the proposed method, we also compare the model parameter size in Table 3. As we can see, the proposed method has a one-third parameter size compared to the baseline. This model can solve the limitations of the baseline method with huge model parameters. With this smaller parameter size, the

TABLE 2
COMPARISON OF METRICS

Metrics	**Case**	**Accuracy**	
		Baseline	**Proposed**
Accuracy	I	0.9877	**0.9984**
	II	0.9898	**0.9926**
	III	0.9772	**0.9868**
Precision	I	0.9877	**0.9984**
	II	0.9899	**0.9927**
	III	0.9772	**0.9870**
Recall	I	0.9877	**0.9984**
	II	0.9898	**0.9927**
	III	0.9772	**0.9866**
F1-score	I	0.9877	**0.9984**
	II	0.9899	**0.9984**
	III	0.9772	**0.9868**

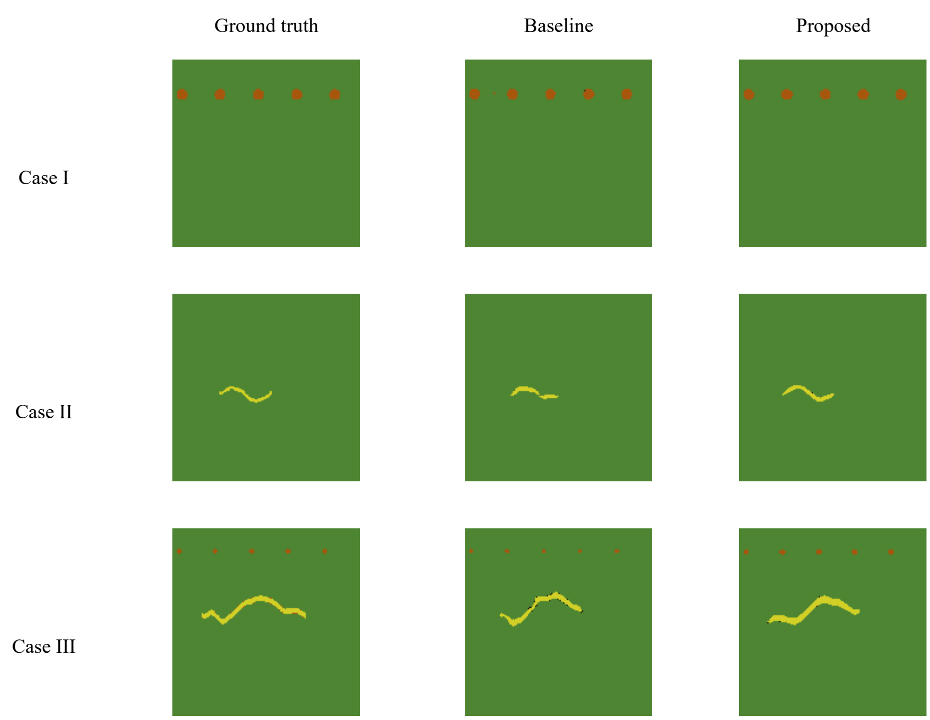

Figure 8. Comparison of inversion result visualization of three observed cases. The colors green, orange, and yellow indicate concrete, rebar, and crack or void, respectively.

TABLE 3
COMPARISON OF MODEL PARAMETER SIZES

Characteristics	Baseline	Proposed
Parameters	61 million	22 million

proposed can be processed faster. Thus, the method is more feasible to be implemented in real-time, especially in the case when complexity and processing time become a concern of the GPR operation.

V. CONCLUSION

In this report, we present our study about the use of a dual-input convolutional autoencoder algorithm for generating the reinforced concrete internal structure visualization from radar data. The method employs the amplitude and phase of the GPR signals. Compared with the baseline method, the proposed method is superior in almost all observed cases. This superiority is also confirmed from qualitative and quantitative perspectives. By its simpler model and superior performance, we show that the proposed method is feasible enough to be applied in real applications. Besides, from this study, we also confirm that the phase information on the recorded radar image is valuable enough for the data inversion aiming at obscured object identification.

In the next stage of the study, more complex conditions, such as the presence of a wet concrete area that can negatively affect the reconstruction results, need to be investigated. Besides, evaluating the real GPR data that may be affected by background noise and interference will confidently confirm its actual implementation.

DECLARATIONS

Conflict of Interest

The authors have declared that no competing interests exist.

CRediT Authorship Contribution

Budiman P.A. Rohman: Conceptualization, Methodology, Visualization; Masahiko Nishimoto: Conceptualization, Methodology; Ratna Indrawijaya: Visualization, Investigation; Dayat Kurniawan: Visualization, Investigation, Writing-Review and Editing; Iman Firmansyah; Writing-Review and Editing; Bagus Edi Sukoco: Investigation.

Funding

Research reported in this publication was supported in part by the Research Organization for Electronics and Informatics, National Research and Innovation Agency under the *Rumah Program Sistem Pendukung Keputusan Berbasis Analisis Citra Satelit* program.

Acknowledgment

The authors would like to thank Kumamoto University for providing experimentation facilities for data generation.

REFERENCE

[1] H. M. Jol, *Ground Penetrating Radar Theory and Applications*. Elsevier, 2008. doi: 10.1016/B978-0-444-53348-7.X0001-4.

[2] A. Benedetto and L. Pajewski, Eds., *Civil Engineering Applications of Ground Penetrating Radar*. Cham: Springer International Publishing, 2015. doi: 10.1007/978-3-319-04813-0.

[3] M. Nishimoto, B. P. A. Rohman, and Y. Naka, “Estimation of concrete corrosion state using ultra-wideband radar signatures,” in *Proc. Int. Geosci. Remote Sens. Symp.*, Jul. 2019, pp. 3610–3613, doi: 10.1109/IGARSS.2019.8899258.

[4] B. P. A. Rohman, M. Nishimoto, and K. Ogata, “Material permittivity estimation using analytic peak ratio of air-coupled GPR signatures,” *IEEE Access*, vol. 10, pp. 13219–13228, Jan. 2022, doi: 10.1109/ACCESS.2022.3147217.

[5] B. P. A. Rohman and M. Nishimoto, “Multi-scaled power spectrum based features for landmine detection using ground penetrating radar,” in *Proc. Int. Conf. Signals Syst. 2017*, May 2017, pp. 83–86, doi: 10.1109/ICSIGSYS.2017.7967075.

[6] S. Busch, J. Van Der Kruk, J. Bikowski, and H. Vereecken, “Quantitative conductivity and permittivity estimation using full-waveform inversion of on-ground GPR data,” *Geophysics*, vol. 77, no. 6, pp. H79-H91, Oct. 2012, doi: 10.1190/geo2012-0045.1.

[7] E. Forte, M. Dossi, M. Pipan, and R. R. Colucci, “Velocity analysis from common offset GPR data inversion: Theory and application to synthetic and real data,” *Geophys. J. Int.*, vol. 197, no. 3, pp. 1471–1483, Jun. 2014, doi: 10.1093/gji/ggu103.

[8] Z. L. Huang and J. Zhang, “Determination of parameters of subsurface layers using GPR spectral inversion method,” *IEEE Trans. Geosci. Remote Sens.*, vol. 52, no. 12, pp. 7527–7533, Dec. 2014, doi: 10.1109/TGRS.2014.2313603.

[9] S. Jazayeri, S. Kruse, I. Hasan, and N. Yazdani, “Reinforced concrete mapping using full-waveform inversion of GPR data,” *Constr. Build. Mater.*, vol. 229, Art. no. 117102, Dec. 2019, doi: 10.1016/j.conbuildmat.2019.117102.

[10] M. T. Pham and S. Lefèvre, “Buried object detection from B-scan ground penetrating radar data using faster-RCNN,” in *Proc. Int. Geosci. Remote Sens. Symp.*, Jul. 2018, pp. 6804–6807, doi: 10.1109/IGARSS.2018.8517683.

[11] K. Dinh, N. Gucunski, and T. H. Duong, “An algorithm for automatic localization and detection of rebars from GPR data of concrete bridge decks,” *Autom. Constr.*, vol. 89, pp. 292–298, May 2018, doi: 10.1016/j.autcon.2018.02.017.

[12] X. Xu, Y. Lei, and F. Yang, “Railway subgrade defect automatic recognition method based on improved faster R-CNN,” *Sci. Program.*, vol. 2018, no. 1, Art. no. 4832972, Jan. 2018, doi: 10.1155/2018/4832972.

[13] Z. Tong, J. Gao, and H. Zhang, “Recognition, location, measurement, and 3D reconstruction of concealed cracks using convolutional neural networks,” *Constr. Build. Mater.*, vol. 146, pp. 775–787, Aug. 2017, doi: 10.1016/j.conbuildmat.2017.04.097.

[14] R. Indrawijaya and B. P. A. Rohman, “Cognitive linear trajectory on GPR imaging using lightweight machine learning,” in *Proc. 2023 Int. Conf. Radar, Antenna, Microwave, Electron. Telecommun.*, Nov. 2023, pp. 436–439, doi: 10.1109/ICRAMET60171.2023.10366779.

[15] J. K. Alvarez and S. Kodagoda, “Application of deep learning image-to-image transformation networks to GPR radargrams for sub-surface imaging in infrastructure monitoring,” in *Proc. 13th IEEE Conf. Ind. Electron. Appl.*, Jun. 2018, pp. 611–616, doi: 10.1109/ICIEA.2018.8397788.

[16] B. Liu *et al.*, “GPRInvNet: Deep learning-based ground-penetrating radar data inversion for tunnel linings,” *IEEE Trans. Geosci. Remote Sens.*, vol. 59, no. 10, pp. 8305–8325, Oct. 2021, doi: 10.1109/TGRS.2020.3046454.

[17] Y. Ji *et al.*, “Deep neural network-based permittivity inversions for ground penetrating radar data,” *IEEE Sens. J.*, vol. 21, no. 6, pp. 8172–8183, Mar. 2021, doi: 10.1109/JSEN.2021.3050618.

[18] S. Yang, *et al.*, “Defect segmentation: Mapping tunnel lining internal defects with ground penetrating radar data using a convolutional neural network,” *Constr. Build. Mater.*, vol. 319, Art. no. 125658, Feb. 2022, doi: 10.1016/j.conbuildmat.2021.125658.

[19] I. Goodfellow, Y. Bengio, and A. Courville, Deep Learning. MIT Press, 2016. Accessed: Aug. 07, 2024. [Online]. Available: https://www.deeplearningbook.org

[20] C. Warren, A. Giannopoulos, and I. Giannakis, “gprMax: open source software to simulate electromagnetic wave propagation for ground penetrating radar,” *Comput. Phys. Commun.*, vol. 209, pp. 163–170, Dec. 2016, doi: 10.1016/j.cpc.2016.08.020.